Continental Shelf Research 31 (2011) 1576–1591

Contents lists available at ScienceDirect

Continental Shelf Research

journal homepage: www.elsevier.com/locate/csr

Research papers

Observations over an annual cycle and simulations of wind-forced oscillations near the critical latitude for diurnal–inertial resonance

P. Hyder [a,*], J.H. Simpson [b], J. Xing [c], S.T. Gille [d]

[a] Met Office, Fitzroy Road, Exeter EX1 3PB, UK
[b] School of Ocean Sciences, University of Wales, Bangor, Menai Bridge, Anglesey LL59 5EY, UK
[c] National Oceanography Centre, Liverpool (formerly Proudman Oceanographic Laboratory), 6 Brownlow Street, Liverpool L3 5DA, UK
[d] Scripps Institution of Oceanography and Department of Mechanical and Aerospace Engineering, University of California, San Diego, La Jolla, CA 92093-0230, USA

ARTICLE INFO

Article history:
Received 17 January 2011
Received in revised form
25 May 2011
Accepted 6 June 2011
Available online 25 June 2011

Keywords:
Diurnal current
Inertial current
Sea breeze
Diurnal wind
Namibia
Benguela current

ABSTRACT

Sea breezes are characteristic features of coastal regions that can extend large distances from the coastline. Oscillations close to the inertial period are thought to account for around half the kinetic energy in the global surface ocean and play an important role in mixing. In the vicinity of 30°N/S, through a resonance between the diurnal and inertial frequencies, diurnal winds could force enhanced anti-cyclonic rotary motions that contribute to near-inertial energy.

Observations of strong diurnal anti-cyclonic currents in water of depth 175 m off the Namibian coastline at 28.6°S are analysed over the annual cycle. Maxima in the diurnal anti-cyclonic current and wind stress amplitudes appear to be observed during the austral summer. Both the diurnal anti-cyclonic current and wind stress components have approximately constant phase throughout the year. These observations provide further evidence that these diurnal currents may be wind forced. Realistic General Ocean Turbulence Model (GOTM) 1-D simulations of diurnal wind forcing, including the first order coast-normal surface slope response to diurnal wind forcing, represent the principal features of the observed diurnal anti-cyclonic current but do not replicate the observed vertical diurnal current structure accurately. Cross-shelf 2-D slice simulations suggest that the first order surface slope response approximation applies away from the coast (> 140 km). However, nearer to the coast, additional surface slope variations associated with spatial variations in the simulated velocity field (estimated from Bernoulli theory) appear to be significant and also result in transfer of energy to higher harmonics. Evidence from 3-D simulations at similar latitude in the northern hemisphere suggests that 3-D variations, including propagating near-inertial waves, may also need to be considered.

1. Introduction

This paper re-examines diurnal currents, which are apparently forced by a resonance between the diurnal wind forcing (i.e. a sea breeze) and the local inertial period of 25.06 h, at a location off the Namibian coast at 28.6°S, 14.6°E (Simpson et al., 2002). The aims of this paper are:

(1) To extend the observations presented by Simpson et al. (2002) to cover a complete annual cycle, and to present new wind observations which, for the first time, allow direct comparison between observed and simulated surface current phases.
(2) To use novel simplified experiments with a 1-D model to gain process insight into the dynamics of rotary diurnal currents forced by diurnal wind stress and its first order surface slope response near a coast, after Craig (1989b).
(3) To make a direct comparison between realistic 1-D process simulations and the observations, particularly the rotary phases, and highlight any differences (that could be evidence of missing 3-D processes such as propagating waves).
(4) To use an idealised simulation from 2-D cross-shelf model to assess the validity of the Craig (1989b) first order approximation for the coast-normal surface slope response to diurnal wind stress.

In this section, we first introduce sea breezes and then inertial resonance to provide background to rather similar wind-forced, tidal and free inertial currents, which often occur simultaneously and need to be carefully distinguished. Next we specifically consider the dynamics of diurnal wind forcing near a coast. In Section 2, we discuss an extended set of observations over a full annual cycle from the same location on the Namibian shelf that

* Corresponding author. Tel.: +44 1392884279.
E-mail address: patrick.hyder@metoffice.gov.uk (P. Hyder).

0278-4343/$ - see front matter
doi:10.1016/j.csr.2011.06.001

was presented by Simpson et al. (2002). In Section 3, we present details of the GOTM 1-D and 2-D cross-shelf slice turbulence closure model configurations used to simulate these currents. Section 4 presents the results from the simulations. Finally, in Section 5, we discuss the results and conclude.

1.1. Sea breezes

Sea breezes are characteristic features of the coastal regions that occur along approximately two-thirds of the earth's coastlines (Simpson, 1994). This daily cycle of generally onshore and offshore breezes results from differential land–sea heating and cooling during the day and night. Sea breezes can be very energetic, for example up to 10 m s^{-1} in the case of the 'Fremantle Doctor' off Western Australia (Pattiaratchi et al., 1997). They have also been observed to extend over 100 km from the coast at several locations (Simpson, 1994; Halpern, 1977; Chen et al., 1996; Gille et al., 2003; Aparna et al., 2005). Due to the earth's rotation, at some locations sea breeze winds rotate until they are approximately coast parallel, particularly at offshore locations.

Gille et al. (2003, 2005) inferred the global variation in the diurnal wind component from the difference between morning and evening wind observed by the QuikSCAT scatterometer (QSCAT). These observations confirm that significant diurnal winds extend far from the coast in many regions offshore and tend to be strongest during summer (Fig. 1). They also suggest that weaker diurnal winds ($\sim$1 m s^{-1} amplitude) can extend thousands of km into the open ocean from the continental coasts. Diurnal changes in the marine boundary layer and the associated effective ocean surface roughness are additional mechanisms that could result in diurnal winds far from land (Barthelmie et al., 1996).

Sea breezes are strong in many regions close to 30°N/S, particularly during summer, due to intense diurnal heating-cooling and the resulting strong land–sea temperature gradients (Fig. 1). Rotunno (1983) and Walsh (1974) present discussions of the linear theory of land and sea breezes which suggests there are fundamentally different resonant responses to diurnal forcing equatorward and poleward of 30°N/S. An interesting question remains as to whether there is an atmospheric resonance between the diurnal forcing and inertial period near 30°N/S. An initial inspection of the global dual scatterometer observations between April and October 2003 (not shown) suggests that the cyclonic diurnal wind rotary components are generally stronger than the anti-cyclonic component. There also appear to several regions of high ellipticity relatively close to the diurnal resonant latitudes. Further work is required to understand this potential resonance. The Namibian and Southwest African coastal regions and seas are known to be regions where sea breezes are strong (Fig. 1) and large land–sea thermal mean temperature gradients also exist (Preston-Whyte and Tyson, 1988; Jury and Spencer-Smith, 1988).

1.2. Inertial resonance

Simpson et al. (2002) and Hyder et al. (2002) present theory of elliptical motion of a surface layer subject to linear friction resulting from diurnal wind forcing for rotary and Cartesian components, respectively. The solutions for clockwise and anti-clockwise forcing at the diurnal frequency were shown to be resonant for the clockwise case at 30°N where $f=\omega$ and for the anti-clockwise case at 30°S ($f=-\omega$). Close to the resonant latitudes the response was shown to tend to the purely anti-cyclonic solution. At these latitudes, a sharp change in the phase of the current response with latitude is also predicted. At latitudes further from 30° the resultant motions become elliptical and both rotary components need to be considered.

The poleward limit of known observations of wind forced rotary diurnal surface currents through diurnal–inertial resonance is in the Aegean at 40°N (Hyder et al., 2002), where $\omega/f\sim0.77$ (inertial period 18.7 h). Hence, from theory, an expected equatorward limit might be 23°S where $f/\omega\sim0.77$ (inertial period $\sim$30.9 h). The resulting regions of expected diurnal–inertial resonance are presented in Fig. 2. Tidal forcing would be expected to result in a similar resonant process (Maas and Van Haren, 1987; Furevik and Foldvik, 1996), although surface slope forcing acts equally through the water column. Assuming the same, ω/f limits, for diurnal tidal periods the resonant regions would be expected to be broadly similar to those for diurnal wind forcing. By contrast, semi-diurnal–inertial tidal resonance might be expected to occur for M2 (period 12.42 h) between 48 and 90°N/S with resonance at $\sim$75°N/S and for S2 (period 12 h) 50–90°N/S with resonance at the pole. However, it should be noted that, since tidal forcing acts through the water column, frictional damping and bottom boundary layer effects would be expected to be more pronounced which could considerably reduce the extent of the tidal resonant regions.

Many documented observations of surface rotary diurnal currents exist in the world's coastal seas (Fig. 2). Several of these observations have been attributed to diurnal wind forcing. Examples of diurnal currents which appear likely to be wind forced are indicated in Fig. 2 with $*$'s: (1) Simpson et al. (2002); (2) Hyder et al. (2002); (3) Chen et al. (1996); DiMarco et al. (2000); Zhang et al. (2010, 2009); Jarosz et al. (2007); (4) Rosenfeld (1988); (5) Hunter et al. (2007); and (6) Lerczak et al. (2001). Candidate observations of diurnal current, temperature or salinity variations that could be wind forced or re-analysed to establish whether they are wind forced are indicated with circles: (7) Simionato et al. (2005); (8) Poulain (1990); (9) Pidgeon and Winant (2005); (10) Kaplan et al. (2005); (11) Rippeth et al. (2002); (12) Pattiaratchi et al. (1997); (13) Halpern (1977); (14) Reynolds-Fleming and Luettich (2004); (15) Pinones et al. (2005); Sobarzo et al. (2010); (16) Kaplan et al. (2003); (17) Kaplan et al. (2003); (18); Schahinger (1988); (19) De Mesquita and Harari (2003); and (20) Zavialov et al. (2002). It should be noted that this database is not comprehensive. It is also possible that some incidences of wind forced diurnal motions are masked by, or have even been attributed to, tidal forcing.

Wind forced anti-cyclonic circular motions have long been known to occur in the surface layers of the ocean (Helland-Hansen and Ekman, 1931). They have been observed and reported in many locations and are particularly pronounced in the absence of friction resulting from strong tidal motion. Recent observations confirm earlier suggestions (Pollard and Millard, 1970; Pollard, 1980, 1970) that near-inertial oscillations comprise around half the kinetic energy in the world's oceans with an energy flux of around 0.5–0.7 TW—a value comparable with that from the internal tide of $\sim$0.9 TW (Park et al., 2005; Watanabe and Hibiya, 2002; Alford 2003a, 2003b; Munk and Wunsch, 1998). Until recently, climate models have tended to use daily coupling between the atmosphere and ocean (Bernie et al., 2007; Danabasoglu et al., 2006) so wind-forced near-inertial energy and associated mixing have not been well represented.

There are two categories of near-inertial motions, with similar dynamics, whereby Coriolis forces drive the radial accelerations. Those with a random phase (in this paper termed 'free' inertial currents) at or close to the inertial frequency are the free motions of water particles in response to impulsive injections of momentum. Those at a specific forced frequency, termed 'periodic', close to the inertial frequency with approximately constant phase are the response to more regular periodic forcing. At many locations both processes can occur. Both mechanisms efficiently transfer energy from the wind to the ocean because of the similar rotary phases of the wind and surface currents since power is given by vector product of wind stress and surface velocity. Near-inertial

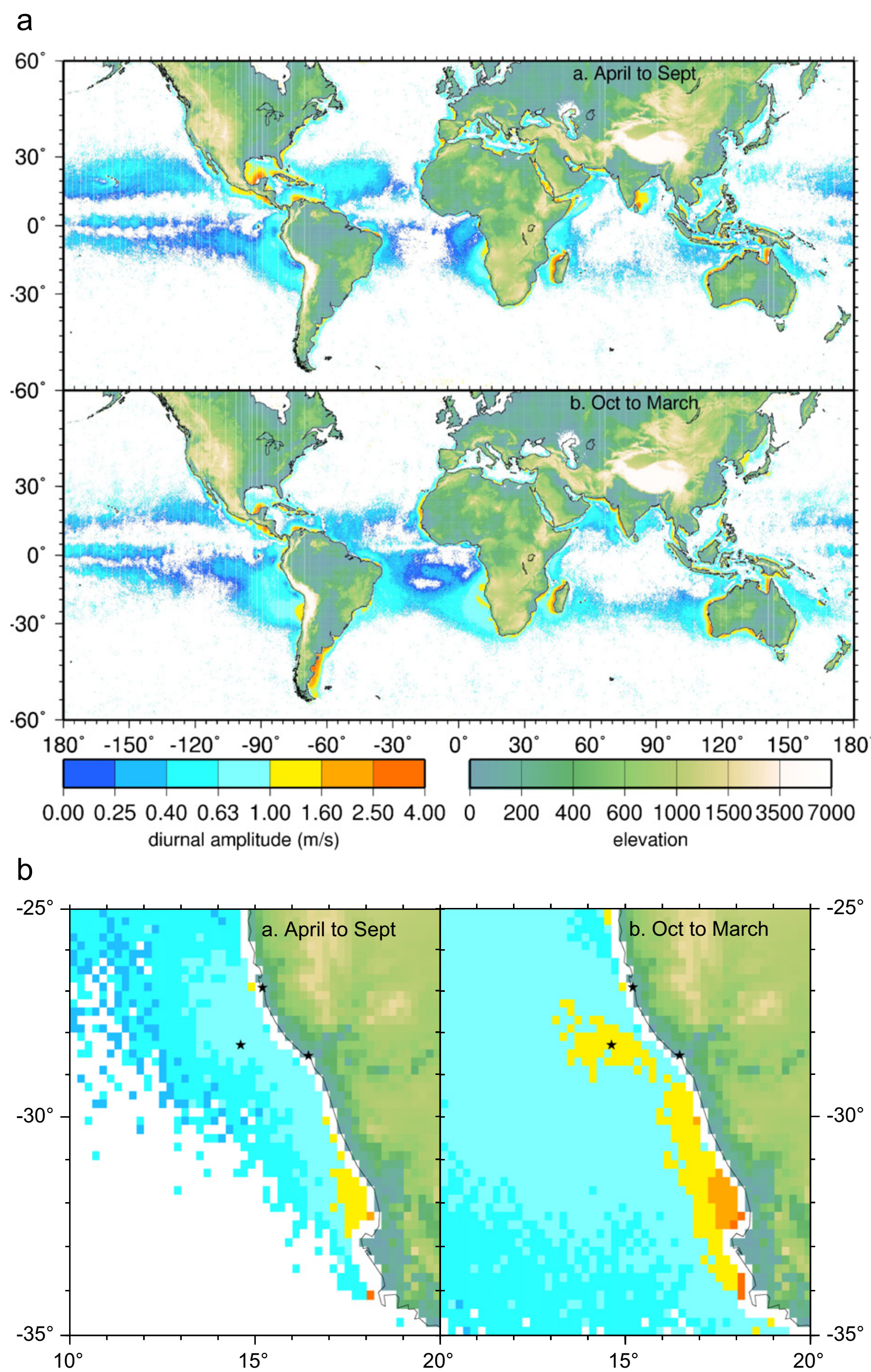

Fig. 1. (a) Estimates of the global variation in the amplitude of the diurnal wind derived from QuickScat (half the difference between morning and evening wind amplitude). Amplitude is simply defined as the vector difference between the morning and evening winds observed from QSCAT averaged over a 7-year period between July 1999 and July 2006 (this represents an extension of the analysis presented by Gille et al., 2003). (b) The region off the SW African coast with the locations of our mooring observations and land-based wind observational stations indicated with black dots.

forcing from intermittent wind events, including intense storms, has been considered by several authors, including a review of observational studies by Price (1981) and a recent modelling study which inter-compares 1, 2 and 3-D model simulations of near-inertial currents off NE Spain by Xing et al. (2004). Craig (1989a, b) present models of periodic wind or diurnal tidally forced current structure close to 30°N and suggest an approximation for the lowest order vertically integrated surface slope response to diurnal wind forcing near to a straight coast. Semi-diurnal tidal resonance with the inertial period has been observed close to 75°N (Furevik and Foldvik, 1996). The propagation of tides near the semi-diurnal and diurnal critical latitudes is discussed by Middleton and Denniss (1993). Van Haren (2005), Simmons et al. (2004) and Simmons (2008) also discuss another mechanism termed sub-harmonic parametric instability, which is thought to concentrate energy from semi-diurnal tides in the near-diurnal energy band at latitudes of 28.8°N/S.

At latitudes which are close to diurnal–inertial resonance, i.e. ~30°N/S, where the diurnal and inertial frequencies are similar, the diurnal–inertial current band can contain energy from both

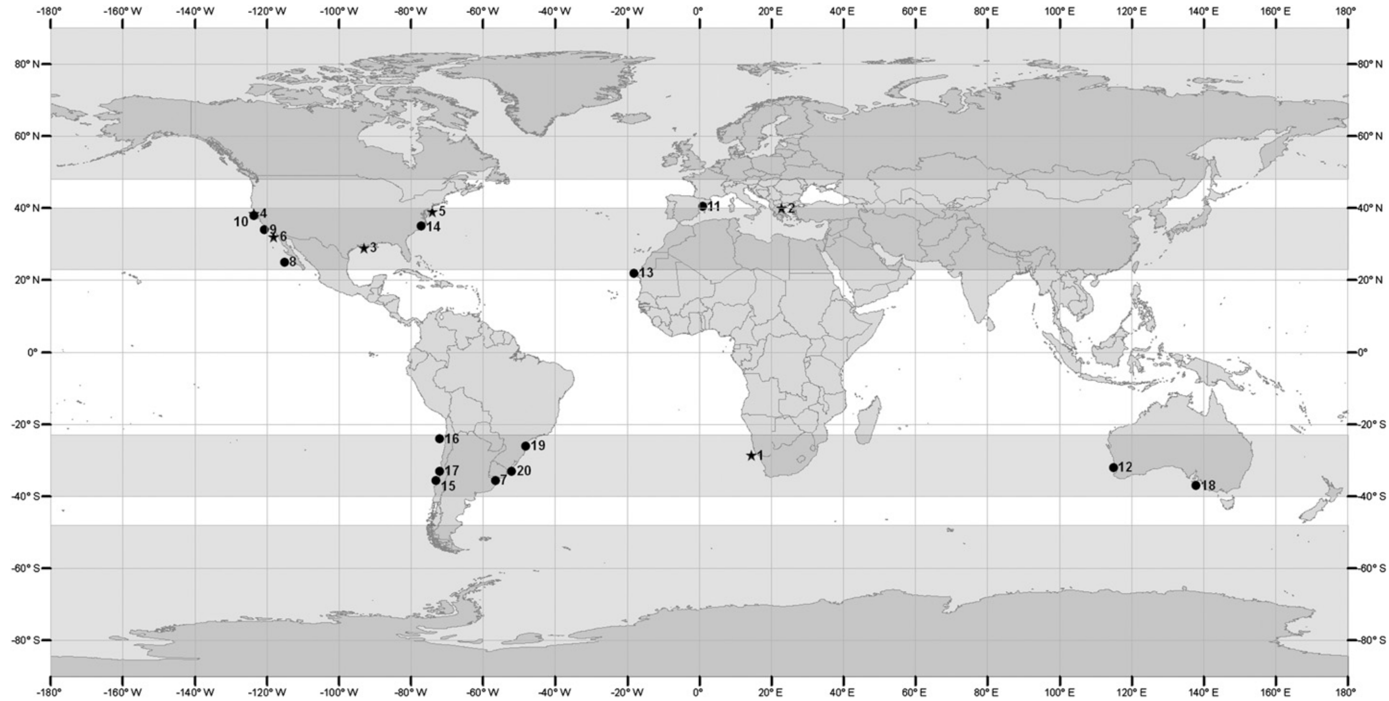

Fig. 2. The equatorward regions where diurnal winds or tidal forcing would be expected to force energetic rotary diurnal currents between 23 and 40°N/S are shaded in grey. The corresponding poleward regions of inertial resonance for semi-diurnal M2 tidal forcing, between 48 and 90°N/S, are also shaded.

impulsive and periodic wind forcing. Further from the resonant latitude, energy has been observed at distinct diurnal and inertial frequencies (Poulain, 1990; Hyder et al., 2002; Rippeth et al., 2002). Unlike the motion resulting from tidal forcing, the motion due to 'periodic' wind forcing might be expected to exhibit some variations in both phase and period due to irregularities in the diurnal wind forcing, thus making it harder to distinguish from either free inertial motion due to impulsive forcing (or from tidally forced motion at similar periods). Furthermore, on relaxation of either impulsive or periodic forcing the motion will immediately revert to free inertial motion. Mean daily cycles, averaged over many cycles, can also help to isolate periodic diurnal wind forced energy from tidally forced or free inertial responses at similar periods (Simpson et al., 2002; Hyder et al., 2002).

1.3. Diurnal wind forcing near a coast

Simpson et al. (2002) present diurnal observations, at the same location considered in this paper, on the Namibian Shelf at 28.6°S (Fig. 3) between March and April 1998 (late summer). A concentration of energy in the anti-cyclonic (anti-clockwise) diurnal band of currents was noted, and evidence of a pronounced anti-cyclonic current component, rotating once per day was presented. A two-layer current structure was observed with rather regular near circular current oscillations. A pronounced phase shift of ~180°, centred on 75 m depth, occurred between the upper layer and the lower layer. Their analysis was extended to include the effect of a coastal boundary. It was hypothesised that in shelf regions a diurnal wind stress in the presence of a coast will produce a diurnal cross-shelf surface slope variation whose magnitude is given by the first order barotropic solution, termed the 'Craig approximation' after Craig (1989b):

$$\frac{\partial \eta}{\partial x} = \frac{\tau_x + i(f/\omega)\tau_y}{\rho g H} \tag{1}$$

where τ_x and τ_y are complex amplitudes such that eastward stress, $T_x = \tau_x e^{i\omega t}$, and northward stress, $T_y = \tau_y e^{i\omega t}$, g is gravitational acceleration, f is the Coriolis frequency, H is the water depth, ω is the diurnal frequency, η is the surface elevation, x is the coast-normal distance offshore and ρ is the water density.

Unlike wind stress, which acts directly only at the surface, the external pressure gradient due the surface slope acts throughout the water column. A simple frictionless two-layer analytical model was developed, in which the upper layer is forced by both the wind stress and the opposing surface slope, whilst the lower layer is forced solely by the surface slope. This simple model predicted the key characteristics of the observed currents.

It should be noted that the dynamic response to wind forced periodic surface slope is very similar to that for the tide, albeit at different frequency. In tidal environments with either free or periodic near-inertial currents, time varying phase differences between upper and lower layer responses, and associated intermittent shear spikes, might be expected and have been observed in a semi-diurnal environment by Burchard and Rippeth (2009).

More recent numerical experiments suggest that near inertial, including sea-breeze, wind stresses can also drive propagating near-inertial waves which can significantly contribute to mixing (Zhang et al., 2010; Xing et al., 2004). A theoretical analysis of coastally trapped near-inertial waves is presented by Dale et al. (2001). Observations of the 3-D structure of near-inertial motions remain, however, rather limited (Zhang et al., 2009; Lewis, 2001).

2. Observations

2.1. Background and methods

A series of measurements was undertaken, covering the period March 1998 to April 1999, by Fugro GEOS for Shell Exploration and Production Namibia B.V., at 28.6°S, 14.6°E. This location is 133 km from the coast at the outer edge of the shelf in water of depth 175 m (Fig. 3). Currents were measured at 4 m intervals every 10 min by upward and downward looking RDI 300 kHz workhorse ADCPs mounted in mid-water. Time is presented as

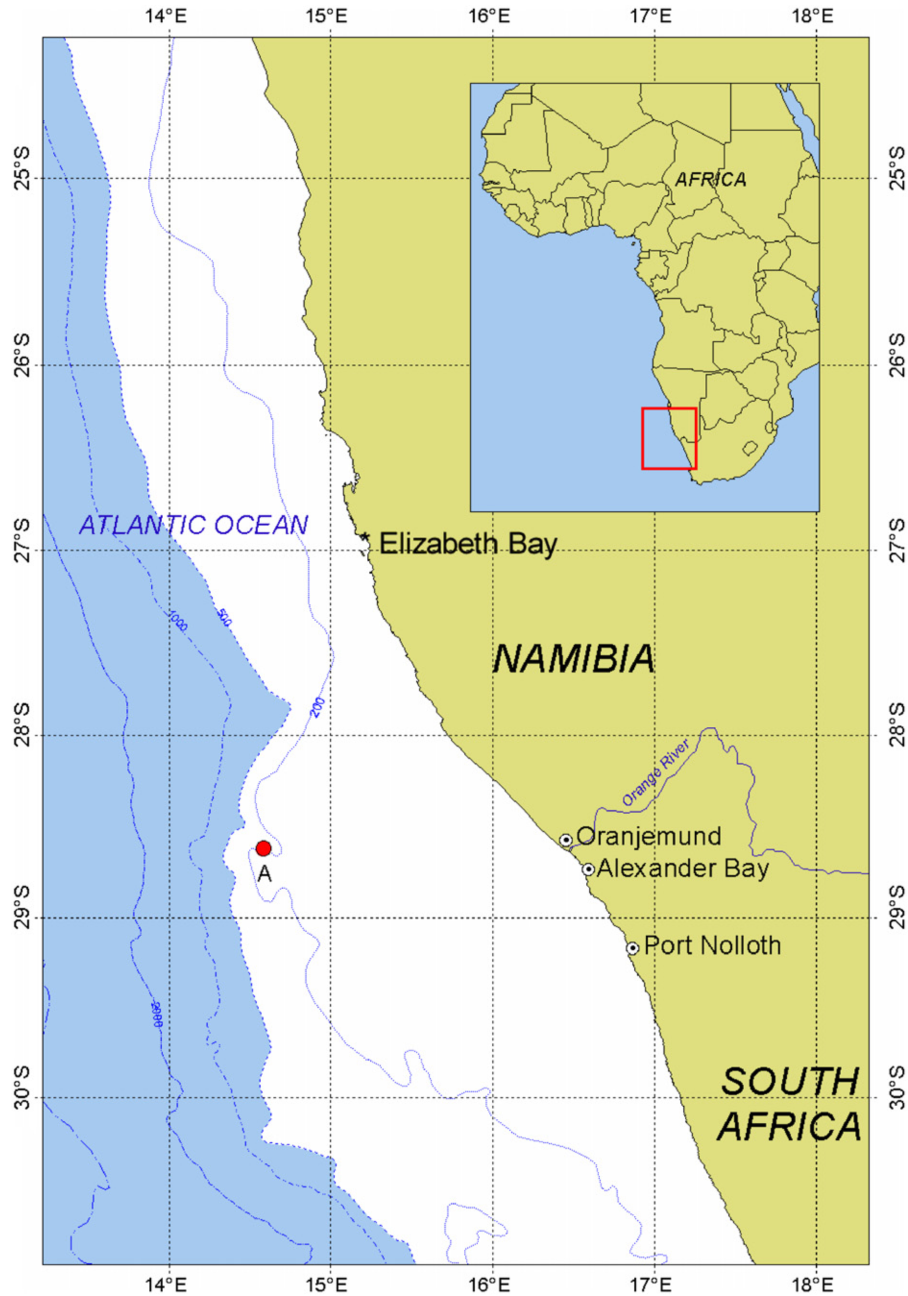

Fig. 3. Location of the observations on the Namibian shelf. The mooring was located in water of depth 175 m close to the outer edge of the shelf.

fractional days since 1 January 1998 00:00GMT. Note Namibia local time is West African Time (GMT+1) between ~3 April and ~3 September and West African Summer Time (GMT+2) between ~4 September and ~2 April. The current data set is complete except during service visits (days 176–178, 302–303 and 358–362) and short period when batteries in both instruments failed due to delays to service visits (days 139–178 and days 293–303 for lower instrument, and days 166–178 for upper instrument). CTD transects between the coast and the mooring location were undertaken at the service visits during March 1998, June 1998, August 1998, December 1998 and April 1999.

Winds were not observed at the mooring location during the mooring deployment period. The nearest source of wind data was at Oranjemund airport (28.6°N, 16.4°E at an altitude of 99 m with a sensor height above ground of 4 m), 150 km to the east of the mooring location. However, these measurements ceased after October 1998 (day 303). The nearest source of wind data covering a full annual cycle was collected at Elizabeth Bay (26.9°N, 15.2°E at an altitude of 15 m with sensor height above ground of 6 m), approximately 200 km to the north of the mooring location (Fig. 3). However, even these wind observations have data gaps between day 162–198, 273–305 and 384–443. A short (20 day) period of wind observations were obtained from a wave scan buoy (with a sensor height of 3 m above mean sea level) close to the mooring location (28.3°S, 14.6°E) during a subsequent observational programme (again on behalf of Shell Exploration and Production B.V.) starting on 20 January 2002, after which the observing buoy was lost.

Using scatterometer satellite wind observations, global estimates of clockwise and anti-clockwise diurnal wind rotation are only possible for the period of the SeaWinds tandem mission, from April to October 2003. For our analysis, we converted wind vectors measured along the satellite swath into wind stress using drag coefficients derived by Yelland and Taylor (1996) and Yelland et al. (1998), as adapted by Gille et al. (2005) for high wind speeds. Following the procedure used by Gille et al. (2005), we averaged all of the available wind stress estimates into $0.25^\circ \times 0.25^\circ$ pixels for 4 times of day corresponding to the satellite overflight times and then least-squares fitted sine and cosine coefficients. Coefficients were converted to clockwise and anti-clockwise amplitudes and phases, and error bars were estimated using a Monte Carlo procedure. For this paper, results are plotted only if the amplitudes exceed the two sigma error bars (i.e., are significant at the $>95\%$ level).

To avoid confusion over the 4 sources of wind information, the reasons for inclusion of each of the sources of wind information are listed below:

- Oranjemund in-situ—to provide time-series of the wind variation at closest land observational site to the mooring location.
- Elizabeth Bay in-situ—to provide a time-series over the full annual cycle of the observational period close to the mooring location.
- Mooring location in-situ (not collocated in time)—to provide the only available information about wind variations at the mooring location.
- Scatterometer remote sensed (not collocated in time)—to provide information of spatial variations in the wind in the region containing the mooring location.

Complex demodulation (Emery and Thomson, 1998) was used to derive the anti-cyclonic and cyclonic amplitudes (A_{ac} and A_c) and phases (ϕ_{ac} and ϕ_c) of the form: $P_{ac}=A_{ac} * e^{i(\omega t+\phi ac)}$ and $P_c=A_c * e^{i(-\omega t+\phi c)}$ for wind, wind stress and current components in time segments of varying lengths. Standard conversion formulae between Cartesian and rotary coordinates are presented by Pugh (1987). Mean daily cycles were calculated by averaging all the available data by time of the day in hourly bins over a full day for the specified periods.

Even with the annual observational record, it remains difficult to automatically distinguish wind-forced motions from tidally forced motions due to their irregular nature and similar periods. Tidal elevations in the region are predominantly semi-diurnal (Lass and Mohrholz, 2005) with a range of 2 m at spring tide (0.6 m at neap tide) (Fugro GEOS, personal communication). The current time-series was analysed using the T_Tide harmonic analysis toolbox. The barotropic (depth mean) and upper layer (21 m) lunar M2 semi-diurnal current major axis amplitude were $\sim$6 and $\sim$8 cm/s, respectively. The barotropic (depth mean) diurnal principal lunar diurnal O1 (period 25.82 h), luni-solar diurnal K1 (period 23.934 h), and principal solar diurnal S1 (period 24.07) major axis amplitudes were $\sim$0.6, 1.4 and 0.6 cm/s, respectively. However, corresponding amplitudes for O1, K1 and S1 for the upper layer (21 m) were $\sim$2, 5 and 12 cm/s. The increased upper layer amplitude in tidal bands close to the diurnal period, in combination with weak barotropic diurnal tides, suggest that there is leakage from the irregular wind-forced near-diurnal band. For this reason, with only a single year of data available we opted to undertake the demodulation on raw current observations, following the approach undertaken by Simpson et al. (2002). This means that any tidal forced diurnal energy will be included in the demodulation analyses. However, one would expect it to be rather weak in view of weak barotropic diurnal tidal signal. The tidal responses would also have different periods, and hence a time varying phases, with respect to wind forced motions.

2.2. Vertical temperature and salinity structure and Benguela (low frequency) current

The vertical variation in temperature, salinity and density during the austral spring (December) and winter (August) are

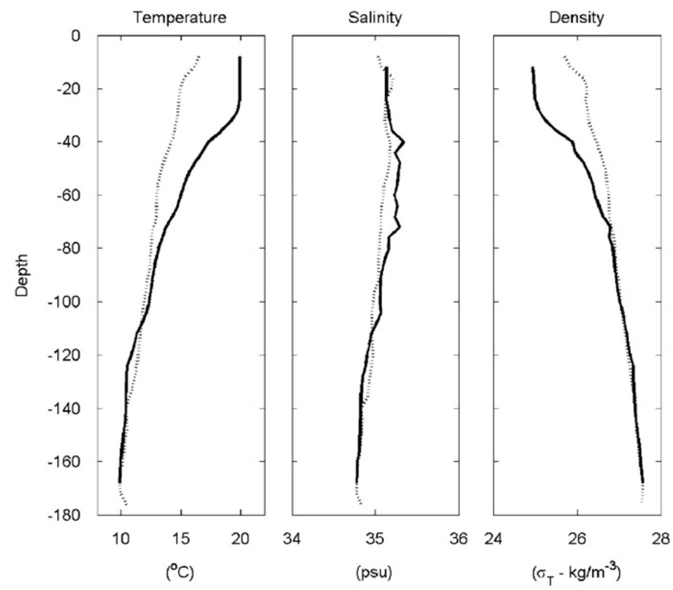

Fig. 4. CTD profiles indicating the vertical structure of temperature, salinity during the austral spring (December 1998) and winter (August 1998) are presented as solid and dotted lines, respectively.

presented in Fig. 4. Stratification was present throughout the year but was stronger during spring when a surface mixed layer of around 30 m depth was observed.

The mooring location is at the southern end of the Benguela upwelling region. Variations in the strength of the Benguela current at 21 and 130 m depth over the annual cycle are presented in Fig. 5. Currents were consistently northward with the predominant current direction being to the northwest. The eastward current component tended to be weaker and more variable than the northward component. Northward current speeds were strongest in the upper water column (20–40 m). The mean annual northward flow of $\sim$0.13 m s^{-1} near the surface decreased approximately linearly with depth to $<$0.02 m s^{-1} at 165 m. There was considerable variability in the exact direction and speed of the current on a range of time scales between 3 and 80 days but no clear seasonal variation was apparent.

2.3. Seasonal variations in diurnal winds and currents

Strong rotary current motions that reverse between upper (0–75 m depth) and lower (75–175 m depth) layers are observed (Fig. 6), as presented by Simpson et al. (2002). The anti-cyclonic and cyclonic diurnal current components (in 48 h segments) over the annual cycle at 21 m (upper layer) and 130 m (lower layer) reveal a clear maximum in the anti-cyclonic diurnal current amplitude in both layers during the austral summer (Fig. 7). As expected, close to 30°S where inertial resonance is expected, the cyclonic (clockwise in Southern Hemisphere) current components are consistently weak.

The anti-cyclonic diurnal wind stress amplitudes also exhibit a seasonal increase during the austral summer. At Oranjemund the amplitudes of cyclonic and anti-cyclonic motions of the wind stresses are roughly equivalent which is indicative of approximately rectilinear diurnal winds (whose phase and alignment are determined by the phases of the anti-cyclonic and cyclonic components). At Elizabeth Bay the anti-cyclonic wind component is generally stronger than the cyclonic component indicating that the sea breeze tends to rotate anti-cyclonically at this location. Note that the different altitudes and sensor heights make it impossible to directly compare observed diurnal wind stress amplitudes between Elizabeth Bay and Oranjemund.

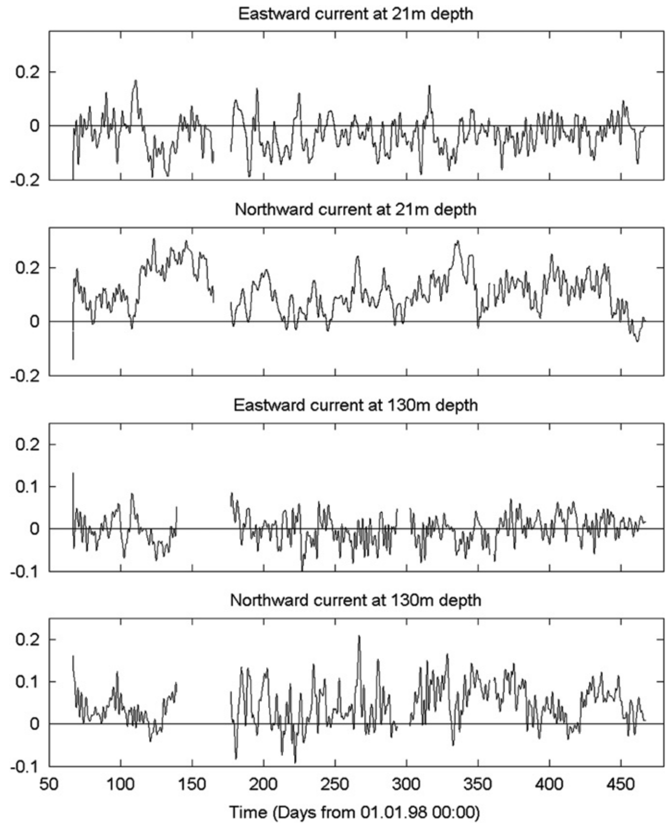

Fig. 5. The annual variation in the low-pass northward and eastward current components at 21 and 130 m depth (from March 1998 to April 1999).

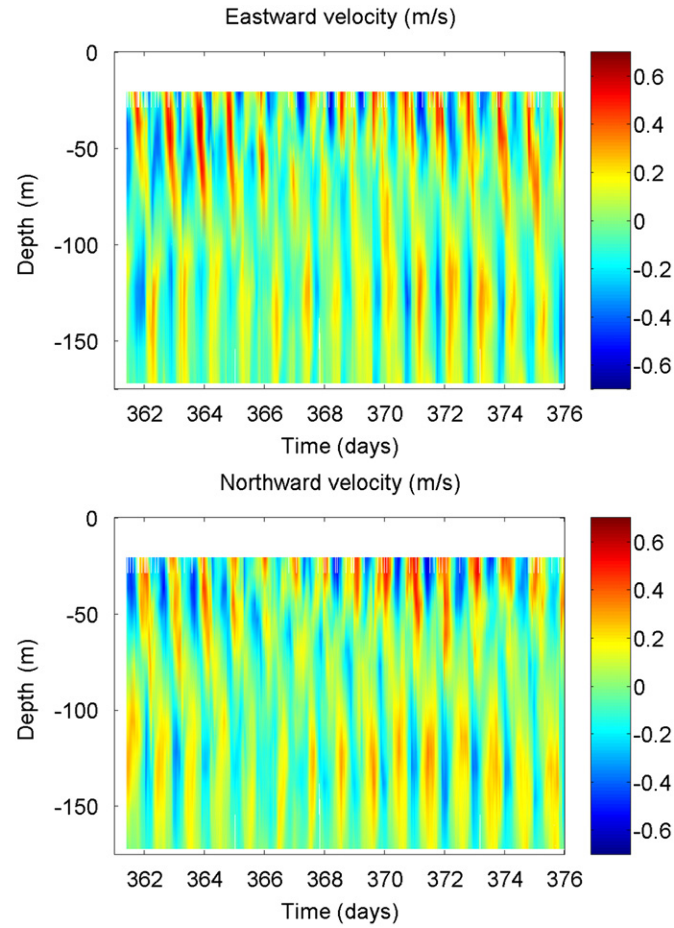

Fig. 6. The observed vertical structure of eastward and northward currents over a fifteen day period from 28 December 1998 00:00GMT to 12 January 1999 00:00GMT. Note these are observed total current with the mean over the 15-day period removed from both current components (i.e. no filtering has been applied).

The corresponding anti-cyclonic diurnal phases are presented as time-series in Fig. 8 and as occurrence histograms in Fig. 9. These figures indicate that in the upper layer the current phases are consistently close to 80° within $\pm 50°$ throughout the annual cycle except during times of weak oscillation (days 80–100, around day 180, days 260–280 and days 300–310). In the lower layer, the current phases are more variable but also have a preferred phase centred at around –129° or 231° ($\sim$209° after the upper layer). The Elizabeth Bay anti-cyclonic diurnal wind stress phase is also relatively constant throughout the year centred on around $199° \pm 70°$. At Oranjemund, the wind stress phase is quite consistent near 220° for the first 50 days (summer) but is more variable after this period. Thus, throughout the year, anti-cyclonic diurnal current in both layers is approximately constant in phase, except for minor phase variations of the same order as those of the anti-cyclonic diurnal wind. Over short periods of relatively weak oscillations (not shown), the diurnal current anti-cyclonic phase tends to increase with time at $15.5°\,d^{-1}$ suggesting that during periods when diurnal winds are weak the motion reverts to the 'free' unforced inertial currents at the inertial period (which at 28.6°S is 25.07 h).

At the mooring location over a 20-day period starting on 20 January 2002 (during the austral summer two years after the simultaneous annual wind and current observations), the diurnal wind stress was 0.010 Pa, i.e. considerably weaker than previously observed at Elizabeth Bay, although the slightly different altitudes and sensor heights should be noted. It also accounted for a lower proportion of the wind variance. At the mooring location, during the later period in early 2002, the anti-cyclonic diurnal wind phase is 118°, i.e. 81° or $\sim$5.5 h, later than for the earlier wind observations at Elizabeth Bay and 38°, or $\sim$2.5 h, earlier than the surface layer current (Table 1).

In order to consider the spatial variation in the diurnal wind stresses we inspect satellite derived diurnal wind stresses. The approximate diurnal wind amplitudes close to Namibia derived from QSCAT, using the method described by Gille et al. (2003), also suggest there is an increase in diurnal wind amplitude during the austral summer (see Fig. 1a, b). Diurnal winds extend far from the coast near the mooring location. It should be noted that the diurnal wind speed amplitude derived from morning minus evening QSCAT wind observations is not directly comparable with the anti-cyclonic diurnal amplitudes that we present from our in-situ observations. Fig. 10. presents the clockwise and anti-clockwise wind stress amplitudes and phases for the period April to October 2003, i.e. the austral winter (the period of the Sea-Winds tandem mission), using the method detailed in Section 2.1. These observational estimates clearly indicate considerable spatial variations in the amplitude and phase of the anti-cyclonic and cyclonic diurnal wind stresses. The estimates of the anti-clockwise phase at the mooring location $\sim$120° are also remarkably consistent with those from the in-situ observations at the mooring location ($\sim$118°). This supports the inference that during the observations the phase of the diurnal anti-cyclonic wind stress at offshore site may have been significantly smaller than (i.e. later or lagging) its phase at the land observing sites. The anti-clockwise wind stress amplitudes are also approximately consistent with those observed at the in-situ location (i.e. considerably weaker than those observed at Elizabeth Bay). However, these satellite

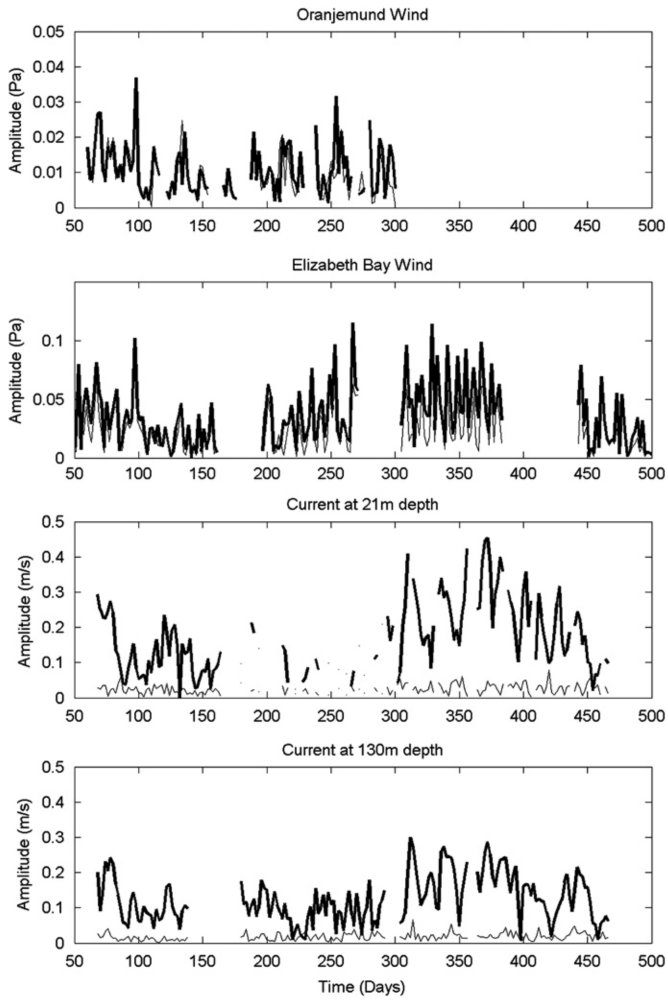

Fig. 7. Seasonal variations in the anti-cyclonic (thick line) and cyclonic (thin line) diurnal wind stress and current amplitudes (observations are between March 1998 and April 1999). Wind stresses are presented for both the Oranjemund and Elizabeth Bay locations. Currents at presented for the upper layer (21 m) and lower layer (130 m).

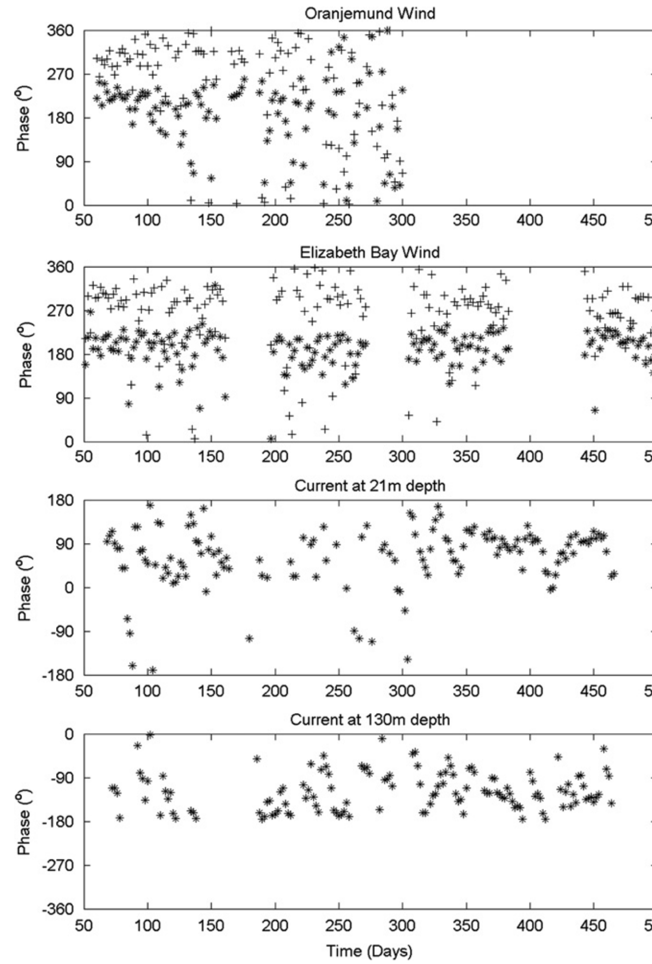

Fig. 8. Seasonal variations in the anti-cyclonic (stars) and cyclonic (crosses) diurnal wind stress and current phase (observations are between March 1998 and April 1999). Winds are presented for both the Oranjemund and Elizabeth Bay locations. Currents at presented in the upper layer (20 m) and lower layer (130 m). Note wind and stress directions are expressed in directions **towards** which the winds are blowing to make them consistent with the currents (but inconsistent with normal meteorological presentation).

observations were during the austral winter when sea breezes would be expected to be weaker.

2.4. Daily cycles of wind and currents and vertical current structure

Some seasonal variations in the vertical structure of these diurnal anti-cyclonic oscillations were evident, as one might expect from seasonal changes in the diurnal wind forcing and stratification. However, despite these variations, both the mean daily cycles and vertical structure of the currents and the daily cycles of the wind are similar over the annual cycle from 11 April 1998 to 11 April 1999 (days 100–465) to those over a 15-day period of strong oscillations between 28 December 1998 00:00GMT and 12 January 1999 00:00GMT (days 361 and 376). The daily cycles of the wind stresses and currents over the annual cycle are presented in Fig. 11. The daily cycles for the period of strong oscillations were also analysed but are not presented graphically. The associated anti-cyclonic fitted wind and current amplitudes and phases for both the annual cycle (days 100–465) and the period of strong oscillations are presented in Table 1, together with those for the subsequent wind observations at the mooring location during 2002 (day 20–40).

Even averaged over a full year clear mean daily cycles in the eastward and northward current and wind stress components were evident. The mean daily current cycles are close to sinusoidal but the wind stress cycles are less sinusoidal indicating the increased importance of higher harmonics in the wind stress daily cycle. At Elizabeth Bay over the annual cycle (and Oranjemund between days 62 and 112), there is a strong northward wind in the late afternoon at 1500GMT. The diurnal fit explains more than 80% of the daily mean wind stress variance and more than 96% of the daily mean current variance (Table 1). The annual mean fitted anti-cyclonic amplitude at Elizabeth Bay was 0.031 Pa. At Elizabeth Bay, the eastward component leads the larger northward component by about 2 h inducing an anti-cyclonic tendency in the wind stress cycle.

Over the period of strong oscillations (days 361–376), the wind and current mean daily cycles were similar to the annual means but their amplitudes were larger by around a factor of two (Table 1). In order to support the analysis of this energetic period, time-series of total wind speeds, total wind stresses and total eastward and northward current at 21 and 130 m between 27 December 1998 and 26 January 1999 (days 360 and 390) are included in Fig. 12. This figure clearly indicates that the mean low frequency wind speed at Elizabeth Bay is to the north and often almost ten times larger than the diurnal component. The wind stress time-series are very irregular with intermittent pulses of strong diurnal energy for short periods of a few days. The figure also demonstrates longer period variability in the diurnal current

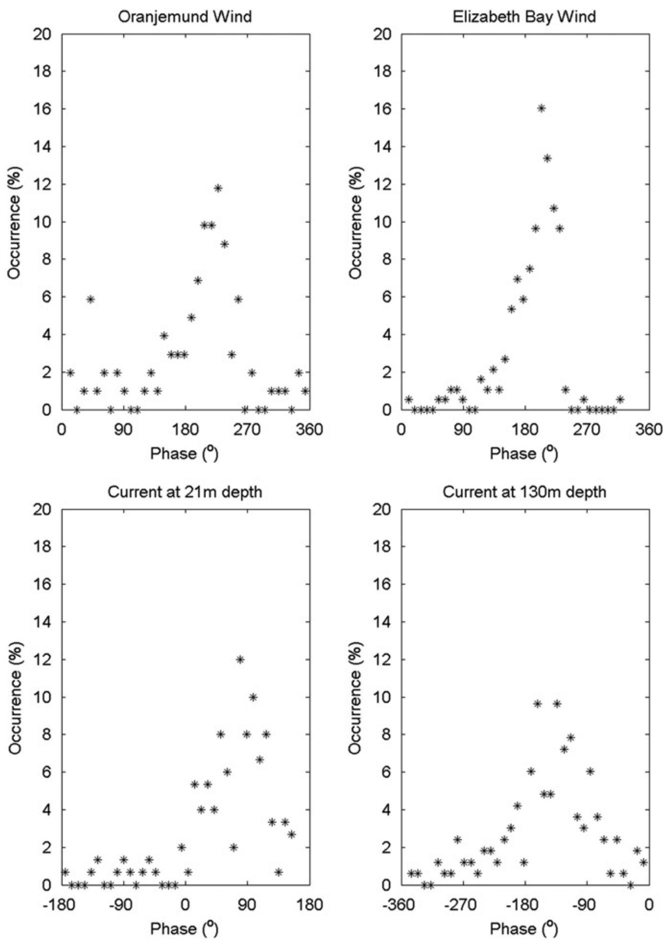

Fig. 9. Diurnal anti-cyclonic current and wind phase occurrence distributions over an annual cycle. Note wind and stress directions are expressed in directions **towards** which the winds are blowing to make them consistent with the currents (but inconsistent with normal meteorological presentation).

amplitudes, at around 10–20 days, which are not evident in the wind observations. This is shorter than the period of the beat frequency $2*pi/(\omega-f)$ which at this latitude is $\sim$23.5 days between two consecutive minima. This $\sim$10–20 period variability in the anti-cyclonic diurnal current is evident through much of the year (Fig. 7).

The vertical structure of the anti-cyclonic diurnal current amplitudes and phases over the period of strong oscillations is presented in Fig. 13. Maximum amplitudes of 0.33 and 0.22 m s^{-1} were observed at 21 m in the upper layer (the uppermost ADCP observation), and at 130 m in the lower layer, respectively. A region of weaker (although non-zero amplitude) oscillations separated the two layers between 60 and 100 m. *Note*: this region is significantly below the upper limit of the thermocline, which is found at around 30 m (Fig. 4). A phase difference of approximately 207° was observed between the anti-cyclonic diurnal phase at 21 m (98°) and 130 m (−109°).

3. Model background

We extend the earlier analysis from simplified 1 and 2 layer analytical models (Simpson et al., 2002) using both the 1-D GOTM model and a 2-D cross-shelf slice model.

3.1. Continuous vertical model with friction (GOTM)

To include the effect of frictional coupling between layers for a stratified water column and bed friction, we consider a large number (100) of layers that are coupled by shear stresses specified in terms of an eddy viscosity. At each level in the model the equations to be solved are:

$$\frac{\partial u}{\partial t} - fv = -g\frac{\partial \eta}{\partial x} + \frac{\partial}{\partial z}\left(Nz\frac{\partial u}{\partial z}\right)$$
$$\frac{\partial v}{\partial t} + fu = -g\frac{\partial \eta}{\partial y} + \frac{\partial}{\partial z}\left(Nz\frac{\partial v}{\partial z}\right) \quad (2a, b)$$

Table 1
Amplitudes and phases of the observed and simulated anti-cyclonic diurnal currents and wind stresses. *Note*: the 2D model results are not included since they are idealised experiments.

Parameter	Diurnal wind or current anti-cyclonic amplitude (Pa or m s^{-1})	Diurnal wind or current anti-cyclonic phase	Explained % of variance by anti-cyclonic plus cyclonic diurnal components for: (A) u/v of raw observations and (B) u/v of daily mean cycle
Annual observations (days 100–465)			
Elizabeth Bay wind stress (Pa)	0.031	199°/13.27 h	(A) 0.21/0.06 (B) 0.87/0.87
Oranjemund wind stress (Pa)—days 62–300	0.004	212°/14.13 h	(A) 0.00/0.04 (B) 0.17/0.81
On location wind stress (Pa) – 2002 – days 20–40	0.010	118°/7.87 h	(A) 0.95/0.08 (B) 0.06/0.00
Current at 21 m (m s^{-1})	0.13	80°/5.33 h	(A) 0.23/0.25 (B) 0.96/0.99
Current at 130 m (m s^{-1})	0.08	−129°/–8.60 h	(A) 0.19/0.21 (B) 0.97/0.99
Oranjemund wind stress (Pa)—days 62–112	0.012	220°/14.67 h	(A) 0.02/0.22 (B) 0.39/0.84
Energetic observations (days 361–376)			
Elizabeth Bay wind stress (Pa)	0.051	209°/13.93 h	(A) 0.39/0.17 (B) 0.85/0.89
Current at 21 m (m s^{-1})	0.33	98°/6.53 h	(A) 0.67/0.74 (B) 0.96/0.98
Current at 130 m (m s^{-1})	0.22	−109°/–7.27 h	(A) 0.73/0.76 (B) 0.99/0.99
Analytical model			
Wind stress (Pa)	0.051	118°/7.87 h	N/A
Upper layer current (0–75 m)	0.25	118°/7.87 h	N/A
Lower layer current (75–175 m)	0.14	−62°/−4.13 h	N/A
Frictional 1D GOTM model			
Wind stress (Pa)	0.051	118°/7.87 h	N/A
Current at 21 m (m s^{-1}, days 60–90)	0.40	38°/2.53 h	N/A
Current at 130 m (m s^{-1}, days 60–90)	0.09	−148°/−9.87 h	N/A

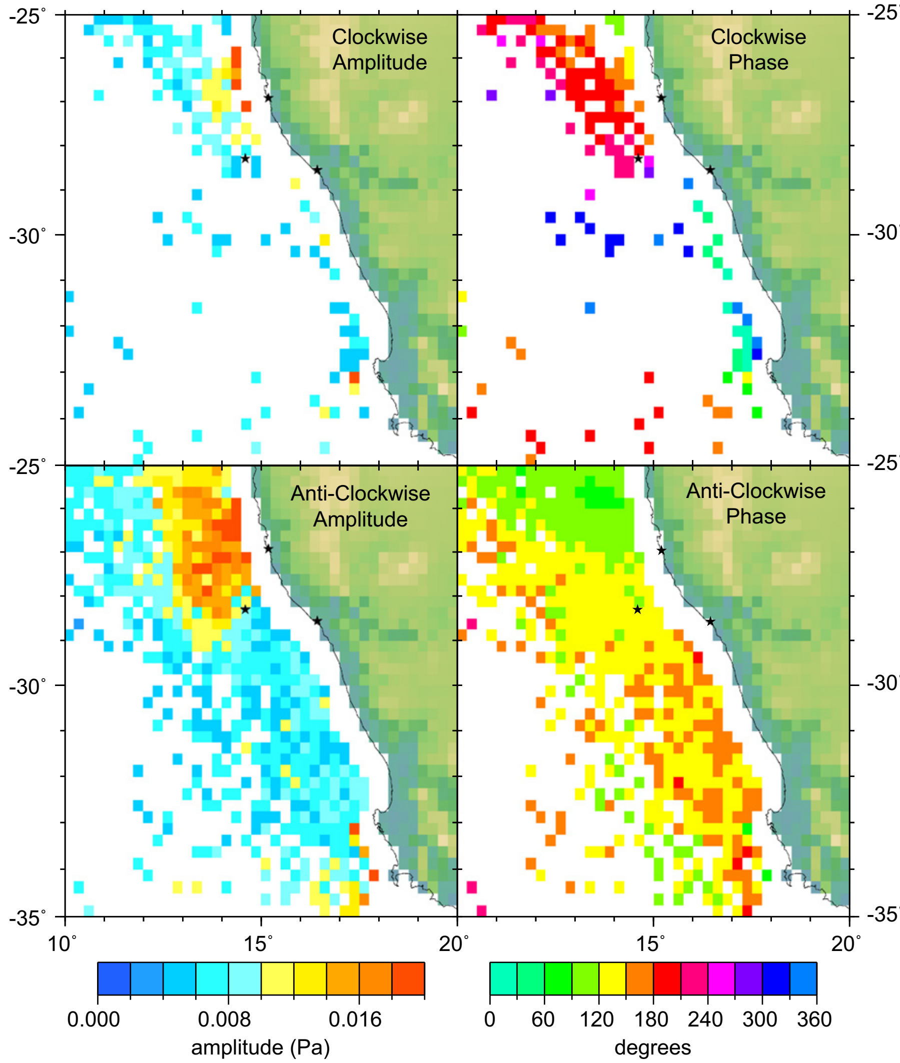

Fig. 10. The spatial variation in the estimated diurnal anti-cyclonic (anti-clockwise) and cyclonic (clockwise) wind stress amplitudes and phases for the SW African region for period of SeaWinds tandem mission (April to October 2003).

We can rewrite Eq. (1) for the first order coast-normal surface slope response to diurnal wind stress in terms of the observed fitted (cosine fit) diurnal wind stress amplitudes, τ_x and τ_y, and phases ϕ_x and ϕ_y:

$$g\frac{\partial \eta}{\partial x} = \frac{|\tau_x|cos(\omega t+\phi_x) - (f/\omega)|\tau_y|sin(\omega t+\phi_y)}{\rho H} \quad (3)$$

Close to the resonant latitude, where $\omega \sim f$, this can be simplified in terms of the anti-cyclonic diurnal amplitude τ_{ac} and phase ϕ_{ac} to:

$$\frac{\partial \eta}{\partial x} = \frac{2\tau_{ac}\cos(\omega t+\varphi_{ac})}{\rho g H} \quad (4)$$

For the idealised experiments, since all of our experiments were between 25°S and 35°S, where f/ω is 1.18 and 0.87, respectively, the $f \sim \omega$ approximation is valid and we considered only the anti-cyclonic wind forcing. At the 28.6°S latitude of the observations f/ω is 1.04 so the approximation is again valid.

To simulate the observed scenarios to account for the alignment of the coastal boundary, as the coast is aligned at -45° relative to north, we add 45° to anti-cyclonic phase of wind and slope forcing. We then subtract 45° from the simulated anti-cyclonic current phase to return to conventional north-south phase reference. For the idealised simulations the coastal boundary was assumed to be aligned north–south so phases were not adjusted.

The model is implemented by integrating Eqs. (2a and b) forward in time using the General Ocean Turbulence Model (GOTM) (Umlauf et al., 2007; Burchard et al., 1998). At the bottom boundary, the stress is specified in terms of a quadratic drag law. Temperature and salinity fields are allowed to evolve through vertical diffusion using diffusivity, K_z, determined by the closure scheme (lateral advection and diffusion are neglected which assumes of spatially uniformity). Unless stated, for all model runs the turbulence closure configuration was the standard set up used for the Irish Sea Liverpool Bay GOTM test case (Umlauf et al., 2007). This includes a second-order Mellor-Yamada closure scheme configured with dynamic dissipation rate and Schumann and Gerz formulations for the stability functions (Umlauf et al., 2007). For standard model runs a minimum turbulence kinetic energy density, $k_{\min}$, value of 1×10^{-6} m^2 s^{-2} was employed. This $k_{\min}$ value is a physically simplified constant value parameterisation used to represent turbulence associated with unresolved or sub grid scale mixing processes, such as internal waves.

The initial state for simulations had all model levels at rest. An exponential taper over the initial ten days was applied to both wind stress and surface slope forcing. Unless otherwise stated the

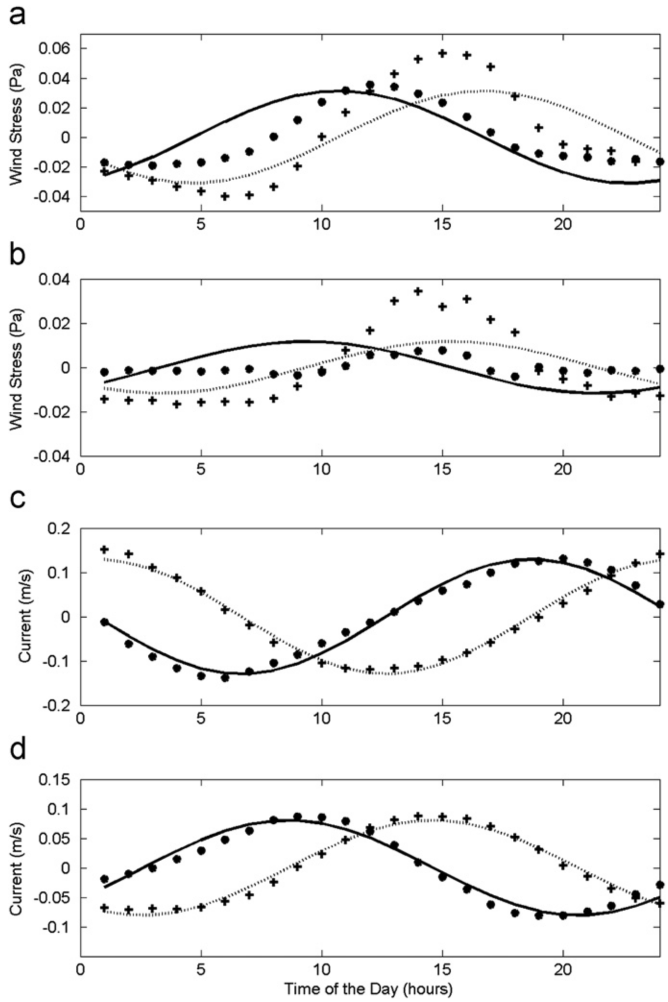

Fig. 11. The mean daily cycles of wind stress and current over the annual cycle from 11 April 1998 to 11 April 1999 (days 100–465). Due to data constraints the daily cycle for wind at Oranjemund is presented for days 62–112. The mean daily cycle of the observations are indicated with symbols (∗ for eastward, + for northward), the anti-cyclonic fits to these observations are indicated with solid and dotted lines, respectively. (a) Elizabeth Bay wind. (b) Oranjemund wind. (c) Current at 21 m depth. (d) Current at 130 m depth.

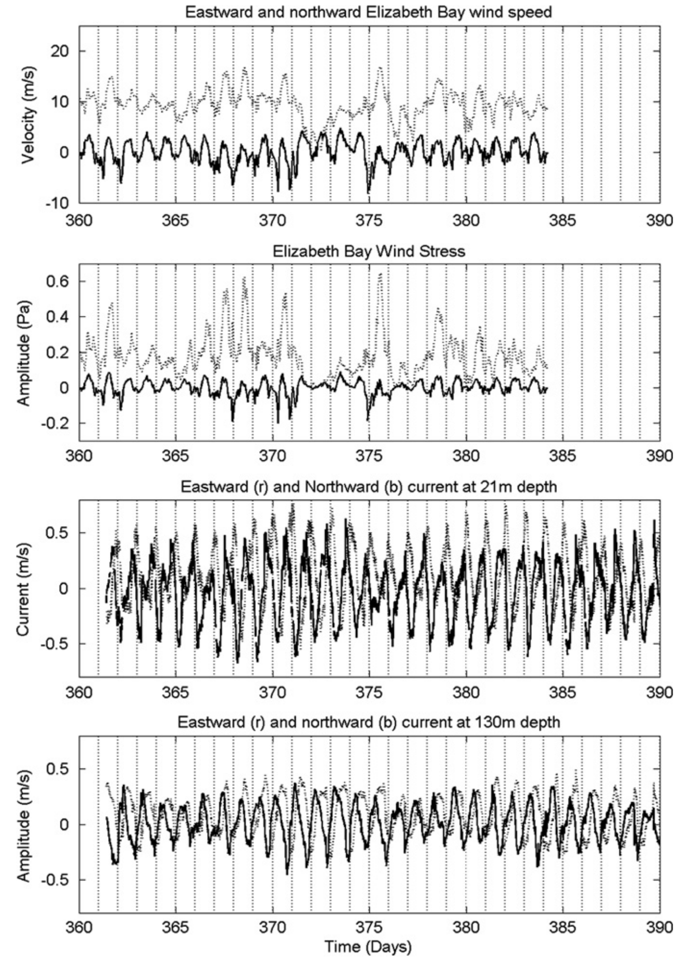

Fig. 12. Time-series of total observed wind speed (Elizabeth Bay), wind stress and current at 21 and 130 m (with mean over the period removed for currents) from 27 December 1998 00:00GMT and 26 January 1999 00:00GMT (days 360–390). Eastward components are presented as solid lines and northward components are dotted lines.

model runs were forced by an anti-cyclonic diurnal wind stress of 0.051 Pa (the observed anti-cyclonic diurnal wind stress amplitude at Elizabeth Bay between 28 December 1998 00:00GMT and 12 January 1999 00:00GMT—days 361 and 376). For the simplified model runs the anti-cyclonic wind phase was set to zero. The model was run forward for 90 days but the complex demodulation was performed over the period from day 60 to 90.

Simplified 1-D simulations were undertaken for a mixed water column and for a water column with linear stratification of 5 °C between the surface and bed at 180 m depth (25 °C surface to 20 °C near bed). Simulations were undertaken for (1) diurnal anti-cyclonic wind stress only, (2) its associated coastal normal surface slope only and (3) both wind and surface slope forcing. These simulations were undertaken at latitudes of 25°S, 30°S and 35°S resulting in a total of 9 runs for each of the stratification cases.

For realistic runs aiming to simulate the observations, the model was initiated using temperature and salinity fields from the CTD observations in December 1998. The anti-cyclonic diurnal wind phase was set to 118°, i.e. the phase of the anti-cyclonic diurnal wind at the mooring location in early 2002. As we do not know the diurnal wind amplitude during the observations, we interpret only relative variations in anti-cyclonic diurnal current amplitudes with depth, i.e. not their absolute amplitude.

3.2. A 2-D cross-shelf model

Both the analytical model and the 1-D GOTM simulations rely on the Craig approximation for the first order sea surface response to diurnal wind forcing near a straight coast. The 2-D cross-shelf model provides a means to assess this approximation. To directly simulate the effects of the coastal boundary, we employ the 2-D cross-shelf model with turbulence closure developed at the National Oceanography Centre, Liverpool (formerly Proudman Oceanographic Laboratory). This model has been successfully used to model other shelf regions (Xing et al., 1999). Details of the model dynamical equations and turbulent closure scheme (Mellor-Yamada level 2.5) are documented in Xing et al. (1999).

The model employs 60 sigma levels, to model a constant depth (150 m) shelf region of width 400 km at 28.6°S. Current data through depth were output between 5 and 395 km from the coast at 10 km intervals. A simple two-layer vertical structure was imposed to promote layer separation ($T=13$ °C for depth > 100 m, $T=15$ °C for depth < 50 m and linear thermal stratification between 50 and 100 m). To investigate the effect of long-shore and cross-shore winds the model was forced with anti-cyclonic wind stress of amplitude 5 m s^{-1} or 0.034 Pa.

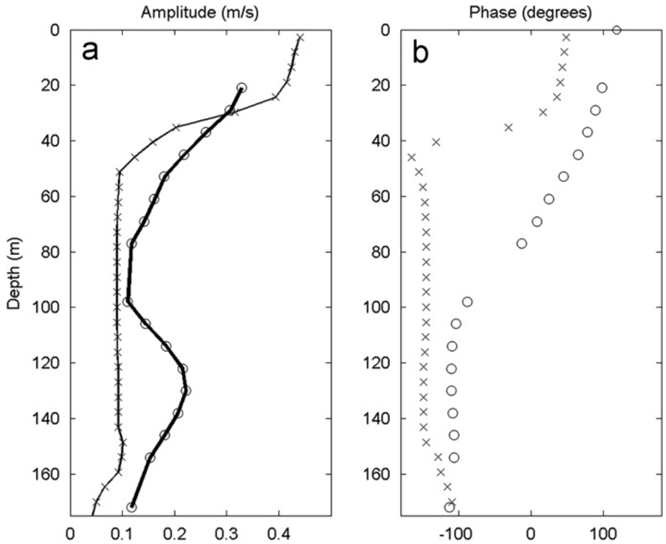

Fig. 13. The simulated diurnal current anti-cyclonic amplitude and phase with anti-cyclonic diurnal wind forcing of 0.051 Pa amplitude at 118° phase and water column stratification as observed in December 1998. Simulations presented include: (a) standard run with $k_{min}=1\times10^{-6}\,m^2s^2$ (*x*); and (b) the observed between days 361 and 376 ('○'s and thick line). Note the phase of the anti-cyclonic diurnal wind stress used to force the model (estimated from observations over a 20-day period from 20 January 2002 at the mooring location) is marked on the *x* axis (i.e. zero depth) with an '○'.

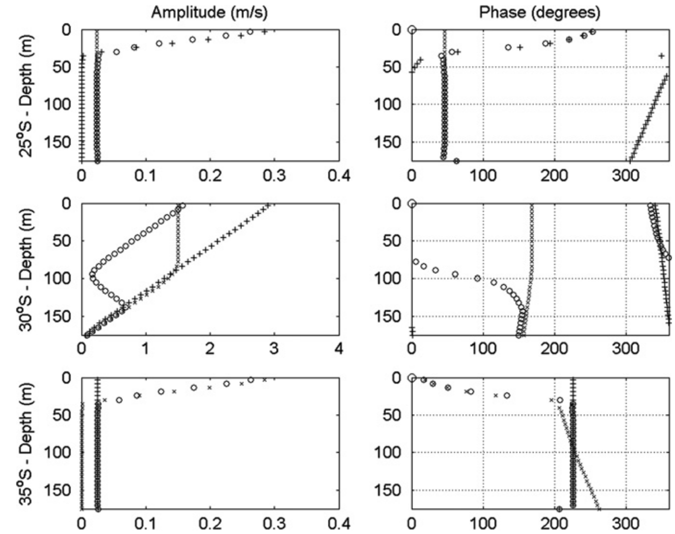

Fig. 14. The GOTM 1-D simulated diurnal anti-cyclonic amplitude and phase for wind and surface slope (○), wind only (*x*) and surface slope only (+) at latitudes of 25°S, 30°S, and 35°S for a water column with approximately linear stratification of 5 °C between the surface (25 °C) and bed (20 °C).

4. Model results

4.1. Simplified 1-D simulations

For the mixed water column, as expected, the anti-cyclonic current responses to either anti-cyclonic wind or its associated surface slope forcing are about 4 times larger at 30°S than at either 25°S or 35°S (not presented as a figure). At each of the three latitudes, however, the response to the wind-forced surface slope forcing is approximately equal but in anti-phase with the wind stress forcing, so the responses to combined wind and surface slope forcing are weak.

For the stratified water column (Fig. 14), the surface response to pure wind forcing is almost ten times larger at 30°S (the resonant latitude) than at either 25°S or 35°S. The penetration of wind energy into the water column, i.e. vertical extent of surface boundary layer, is also considerably greater near resonance at 30°S than at 25°S or 35°S (as documented by Craig, 1989a, b). At the resonant latitude the phase (lead) of anti-cyclonic current is fairly constant with depth. Poleward of this latitude, the phase increases with depth, and equatorward of this latitude, the phase decreases with depth. The phase of the surface current response to the anti-cyclonic wind only also varies strongly with latitude. For surface slope forcing only, the anti-cyclonic current response is more than five times more energetic at the resonant latitude than at 25°S or 35°S. As expected, the anti-cyclonic diurnal current phase at each site is approximately constant with depth but again varies considerably with latitude. As expected, the extent of the bottom boundary layer is considerably enhanced at the resonant latitude. Wind and slope forcing with stratification results in an approximately two-layer current structure with phase reversal between layers (as expected from the analytical model). At the resonant latitude, the extended boundary layers result in a second lower layer maximum in the anti-cyclonic current amplitude. Further from the resonant latitude, the upper layer is shallower and weaker, and the lower layer response is of approximately constant amplitude.

4.2. Realistic 1-D model simulations

The realistic simulations, with the assumed phase of ~118°, provide reasonable qualitative representation of the observed anti-cyclonic diurnal vertical current structure, particularly the two-layer current structure with phase reversal between the layers (Fig. 13). However, several key differences between the simulated and observed vertical diurnal anti-cyclonic current structure exist: the upper layer depth is shallower than observed for the period of strong oscillations; the relative amplitude of the upper layer flow relative to the lower-layer flow is too high (possibly, at least in part, as the result of the upper layer being too shallow); there is no sub surface amplitude maximum in the lower layer; and the vertical variation in phase of the simulated anti-cyclonic diurnal current is rather different to that observed. The amplitudes and phases of the upper and lower layers from the observations, the analytical model and the realistic simulations are presented in Table 1.

For the period of strong oscillations, the diurnal anti-cyclonic phases of the upper and lower layer currents are 98° and –109°, respectively (the corresponding values are 80° and −129°, respectively, over the annual cycle). Given the observed layer depths, the frictionless two-layer analytical model, presented by Simpson et al. (2002) predicts upper layer current, and lower layer current phases of 118° and –62°, respectively. The GOTM 1-D model predicts corresponding phases of 38° and −148° for period of strong oscillations. There is therefore an observed lag of 20°, for the period of strong oscillations between the wind (not co-located in time) and upper layer current. For the 1-D model this lag is 80°, which represents an apparent error of 60° or 4.0 h. It should be noted both that the diurnal a/c wind phase at the mooring during the observations is not known and that the variations in the phase (±70° or 4.7 h) of the diurnal wind at Elizabeth Bay (Figs. 8 and 9) are larger than the above-mentioned phase error. Note also that the analytical model requires the observed layer depths as inputs whereas the vertical current structure is simulated by GOTM.

Given the observed layer depths, the frictionless two-layer analytical model predicts upper and lower layer diurnal anti-cyclonic current amplitudes for the period of strong oscillations of 0.25 and 0.14 m s^{-1}, respectively, i.e. with a similar amplitude ratio to those observed of 0.33 and 0.22 m s^{-1}, respectively. By contrast the 1-D realistic frictional simulations produced upper and lower layer currents of amplitude 0.40 and 0.09 m s^{-1}, respectively.

Despite the ten-day exponential taper for all forcing, significant beating in the oscillatory current components is observed with a timescale of around 25 days between consecutive maxima or minima (not shown as a figure). This is similar to the expected beat frequency of $2*pi/(\omega - f)$ which at this latitude is around 23.5 days but longer than the observed beat period of 10–20 days. This beating results in an oscillation in the apparent anti-cyclonic diurnal phase (for our complex demodulation with a 48 h window) of $\sim \pm 50^\circ$. This beating persists for more than 500 days and appears to be related to the decay of inertial energy from the initial exponential taper to the diurnal wind stress.

The apparent errors in the simulated vertical structure, in particular, the too shallow upper layer depth and too strong amplitude, are very interesting. They could arise either because the simulated downward transfer of wind forced momentum is too small or because the relative magnitude of diurnal wind and slope forcing for the model is not correct, i.e. the Craig approximation is invalid. The downward transfer of wind momentum is controlled by the mixing, which in turn depends on the stratification and shear and, in consequence, latitude, as well as unresolved 3-D processes such as internal waves. The sensitivity of the upper layer thickness and amplitude to latitude in our idealised 1-D simulations should be noted.

An additional series of modified simulations were therefore undertaken (not presented as figures). These included: (a) employing a mean coast normal pressure gradient to force a mean flow with a surface speed of $\sim$0.5 m s^{-1}; (b) employing wave induced surface turbulence injection (Umlauf et al., 2007); (c) employing an unrealistic minimum TKE of 1×10^{-3} m^2 s^2 to represent a large unknown unresolved mixing source; (d) adjusting the latitude and effective inertial period from 27.4° to 29.6° to crudely represent the effect of background vorticity due to horizontal mean flow shear, estimated from a GCM; and (e) changing the water depth to change relative magnitude of slope forcing compared to wind forcing. Experiments (a), (b), (d) and (e) did not significantly improve the agreement between the simulated vertical structure and the observations. Experiment (c) provided much better representation of vertical phase variation, deepening the upper layer depth to around 60 m and reducing the error in the lag between the wind and upper layer (21 m) current by around 30° or 2 h.

4.3. Cross-shelf 2-D slice model simulations

The variation in the diurnal anti-cyclonic component of elevation and coast normal surface slope with the distance from the coast simulated using the 2-D cross-shelf model forced by pure anti-cyclonic winds is presented in Fig. 15. Towards the outer shelf (> 147 km from the coast) the diurnal surface slope amplitudes tend towards the value predicted by the first order Craig approximation. This was also confirmed for the simulations with either purely alongshore or purely cross-shore diurnal winds. However, closer to the coast (< 147 km), the diurnal slope amplitude exhibits considerable variations with distance from the coast. In this region, significant semi-diurnal variations in the slope are also evident, which result in significant amplitude semi-diurnal oscillatory currents (Fig. 15). Semi-diurnal, surface current amplitudes are smaller than diurnal current amplitudes by a factor of $\sim$5. Both the semi-diurnal and diurnal currents tend to rotate anti-cyclonically but the relative amplitude of cyclonic component compared to anti-cyclonic component is lower for the diurnal frequency. Very close to the coast, as expected, cyclonic and anti-cyclonic amplitudes tend towards equal values, i.e. rectilinear flow, since flows are confined to be coast parallel.

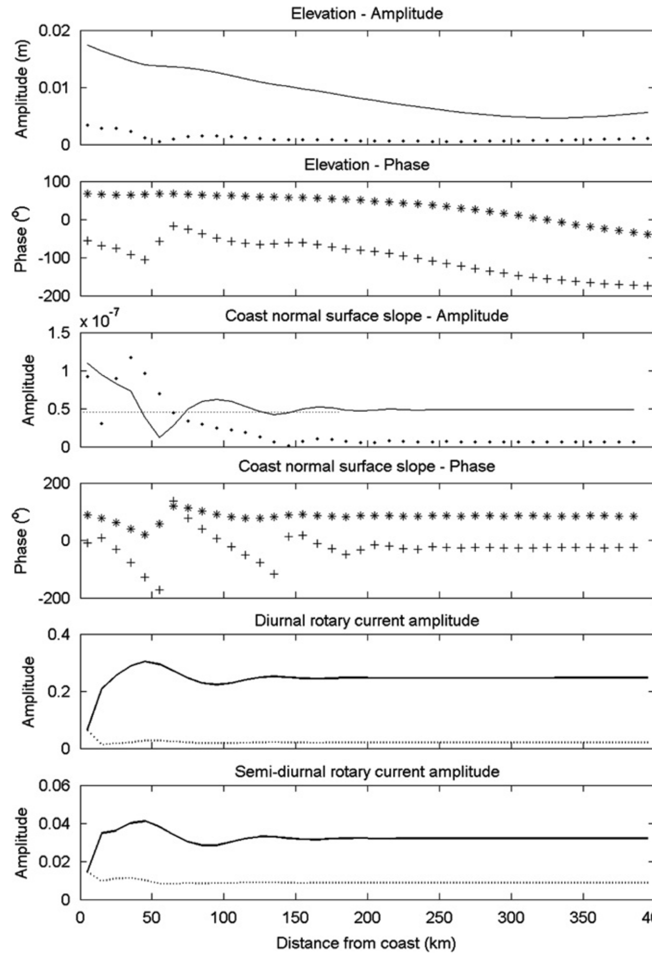

Fig. 15. Cross-shelf variations in diurnal (solid lines for amplitude and $*$s for phase) and semi-diurnal (dotted lines for amplitude and +s for phase) amplitude and phase of surface elevation and slope simulated by the 2-D cross-shelf model (sine fit using least square). The coast-normal diurnal surface slope amplitude predicted using the Craig approximation is also indicated with a black dashed line. Also included are the surface rotary diurnal and semi-diurnal current anti-cyclonic (solid line) and cyclonic (dotted line) amplitudes.

The occurrence of both spatial variations in diurnal and non-zero semi-diurnal coast normal surface slopes suggest that a second-order process must influence the surface slopes in addition to first order response to diurnal wind stress. From Bernoulli theory (Kundu and Cohen, 2002), for quasi-steady motion, the gradient in the Bernoulli function, B, is given by

$$\nabla \underline{B} = \underline{u} x \underline{\omega} = \nabla(0.5q^2 + p/\rho + gz) \tag{5}$$

where $\underline{\omega}$ is $\nabla\ x\ \underline{u}$, q is $|\underline{u}|$, p is external pressure forcing, g is acceleration due to gravity and z is the vertical location in the fluid. Neglecting the vertical velocity, w, and all $\delta/\delta y$ terms gives:

$$\underline{u} x \underline{\omega} = (v\partial v/\partial x, -u\partial v/\partial x, u\partial u/\partial z + v\partial v/\partial z) \tag{6}$$

Evaluating gradients in the x and y directions along the surface (i.e. $z = \eta$) and assuming atmospheric pressure is spatially uniform gives

$$\frac{\partial \eta}{\partial x} = v\frac{\partial v}{\partial x} - \frac{\partial}{\partial x}\left(\frac{q^2}{2}\right) \tag{7}$$

and

$$\frac{\partial \eta}{\partial y} = -u\frac{\partial v}{\partial x} - \frac{\partial}{\partial x}\left(\frac{q^2}{2}\right) \tag{8}$$

It should be noted that Bernoulli theory is simply a way of presenting the inviscid momentum equations assuming that

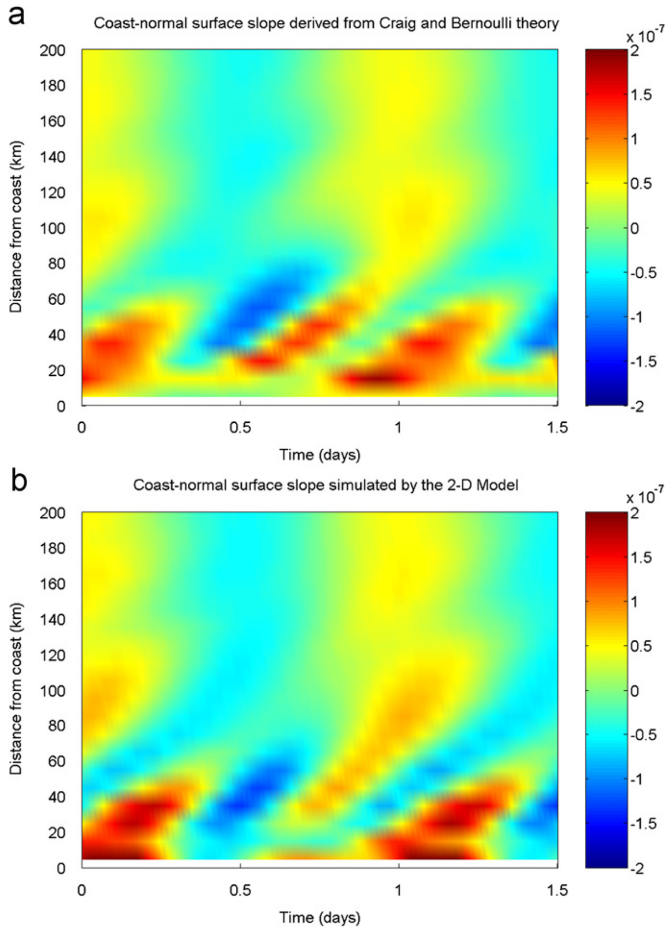

Fig. 16. The cross-shelf and temporal variations in the surface slope (a) derived from the wind stress using the Craig approximation together with those derived from the simulated velocity fields using Bernoulli theory; and (b) simulated by the 2-D cross-shelf model.

gravity is the only body force (i.e. neglecting bed friction and Coriolis). Hence, equivalent equations could be directly derived from the inviscid equations of motion (Euler equations) by making the same assumption of quasi-steady flow and ignoring bed friction, rotation and surface stresses.

Using the simulated velocities from the 2-D model it is possible to estimate the terms in Eq. (7) for the coast normal surface slopes derived from Bernoulli theory. These can then be added to the first order estimate from the Craig approximation to provide an estimate of the expected coast normal sea surface slope variations in the simulation. The variations in coast normal surface slope predicted by Bernoulli theory, in combination with Craig theory, are qualitatively similar those in the direct simulations (Fig. 16). In particular, the non-linearities in the frictionless Bernoulli equations appear to result in significant semi-diurnal sea surface slope variations (in our 2-D model which is forced only with diurnal winds). However, one should also note the differences between the estimates and simulated surface slopes (Fig. 16), which suggest that some of the assumptions in the Bernoulli theory are only partially valid.

5. Discussion

In summary, new observations and simplified models of increasing complexity have been used to gain insight into the dynamics of the observed diurnal anti-cyclonic currents off the Namibian coast. Key results are discussed below.

5.1. New observations

The approximately constant anti-cyclonic diurnal wind and current phases throughout the year suggests both winds and currents are very close to the diurnal frequency. Barotropic tidal currents are also weak. The observed diurnal currents therefore do not appear to result from either lunar tidal forcing or the sub-harmonic parametric instability mechanism, which is thought to concentrate near-diurnal energy at latitudes of 28.8°N/S (Simmons, 2008; Simmons et al., 2004; Van Haren, 2005). The observed maxima in both the diurnal anti-cyclonic wind and current amplitudes during austral summer could also suggest that they may be wind forced.

The anti-cyclonic diurnal wind exhibits large irregular day to day variations with intermittent short periods of very strong diurnal winds. The anti-cyclonic diurnal current amplitudes are generally more regular (as one might expect from a response with low friction) but appear to exhibit longer period variations on periods of 10–20 days. This oscillation is shorter than the expected (and 1-D simulated) beat period between oscillations at the diurnal and inertial frequencies of ~23.5 days but could also result from periodicity in the irregular diurnal wind forcing and/or modification of diurnal–inertial beat period by background vorticity in the 3-D mean flow structure.

New wind observations from both the current mooring location (January to February 2002) and from analysis of scatterometer satellite wind observations (April to October 2003) provide evidence of strong spatial variations in the diurnal anti-cyclonic wind stress over relatively short distances and suggest the diurnal wind phase at the mooring location is normally ~118° (i.e. 81°, or ~5.4 h, later than the corresponding phase of the Elizabeth Bay annual (days 100–465) wind observations).

5.2. 1-D model experiments

Our simplified 1-D experiments have provided process insight into the diurnal–inertial resonance. They have demonstrated the marked sensitivity, when close to resonance, of the vertical structure and, in particular, upper layer thickness to latitude. The realistic 1-D model simulates diurnal currents, which are qualitatively similar to those observed. In particular, the simulated phase lag between the wind forcing and the upper layer (21 m) current agrees with those observed over the annual cycle and period of strong oscillations to within 60° or 4 h. This represents reasonably good agreement, given the lack of co-located simultaneous wind observations and observed variability in diurnal wind phase of ±70° or ~5 h. This provides increased evidence that the motions are principally wind-forced.

The vertical structure of simulated diurnal anti-cyclonic amplitudes and phases is, however, significantly different to that observed. In particular, the upper layer depth is too shallow and the upper layer amplitude is too strong. This could suggest our 1-D simulations are missing an important source of mixing such as internal waves. However, in view of the above-mentioned sensitivity of the upper layer thickness and response to latitude, it could also arise from background vorticity in the 3-D mean flow structure. Novel 3-D numerical experiments documented by Zhang et al. (2010) suggest propagating near-inertial Poincare waves may occur from diurnal wind forcing equatorward of the resonant latitude and result in enhanced mixing near the resonant latitude. This provides evidence that important sources of mixing might be expected to be missing from our realistic 1-D experiments.

5.3. 2-D model experiments

The idealised 2-D cross-shelf slice simulations suggest that the Craig approximation for the first order barotropic surface slope response to diurnal wind stress in the presence of a coast is valid far (>150 km in this simplified case) from a straight coast. However, they also suggest that closer to the coast, cross-shore variations in diurnal and semi-diurnal coast-normal surface slope resulting from spatial variations in the velocity field due to the coastal boundary need to be considered. These slope variations result in cross-shelf variations in the anti-cyclonic diurnal current structure and induces significant semi-diurnal currents in the region close to the coast (<50 km in this case). The main variations in the coast normal surface slopes are qualitatively predicted by combining the slopes estimates by the Craig approximation with those estimated by Bernoulli theory. This Bernoulli non-linearity mechanism for energy transfer to higher harmonics is expected to apply generally (and is independent of any non-linear energy transfer that might result from bottom friction, irregular depth or internal friction). Note again that Zhang et al. (2010) simulations suggest 3-D propagating near-inertial waves should also be considered.

5.4. Conclusions and future work

In combination, these results provide considerably increased confidence in our earlier hypothesis (Simpson et al., 2002) that these oscillations may be forced by the diurnal wind stress in the presence of the coast. Co-located spatial wind, current and vertical structure and turbulence observations are essential to further investigate the apparent discrepancies between these simplified models and the observations. 3-D modelling would also be valuable to investigate the 3-D nature of these oscillations, including any propagating components of the diurnal or near-inertial response, as simulated by Zhang et al. (2010). The spatial variations in the observed diurnal wind stress and water depth would be expected to result in significant spatial variations in the current responses, which might be expected to drive propagating motions, through their associated convergent and divergent flows, and increase vertical mixing.

Acknowledgements

We would like to thank Chris Shaw and Jon Upton (Shell Exploration and Production B.V.) and Shell Exploration and Production, Namibia, B.V. for making this valuable data set available for scientific research. Thanks also to Fugro GEOS who undertook the observations and to John Siddorn (Met Office) for providing valuable comments on the final draft manuscript. This manuscript benefited considerably from comments from two anonymous reviewers. STG acknowledges support from NASA contract NNX08AI82G.

References

Alford, M., 2003a. Improved global maps and 54-year history of wind work on ocean inertial motions. Geophysical Research Letters 30. doi:10.1029/2002GL016614.

Alford, M., 2003b. Redistribution of energy available for ocean mixing by long range propagation of internal waves. Nature 423, 159–162.

Aparna, M., Shetye, S., Shankar, D., Sheinoi, S., Mehra, P., Desai, R., 2005. Estimating the offshore extent of sea breeze from QuikSCAT scatterometry. Geophysical Research Letters 32 (13), 1–4. doi:10.1029/2005GL023107 (L13601).

Barthelmie, R., Grisogono, B., Pryor, S., 1996. Observations and simulations of diurnal cycles of near surface wind speeds over land and sea. Journal of Geophysical Research 101 (16), 21,327–21,337.

Bernie, D.J., Guilyardi, G., Madec, G., Slingo, J.M., Woolnough, S.J., 2007. Impact of resolving the diurnal cycle in an ocean atmosphere GCM: part 1: a diurnally forced OGCM. Climate Dynamics 29, 575–590.

Burchard, H., Petersen, O., Rippeth, T.P., 1998. Comparing the performance of the Mellor-Yamada and the κ–ε two-equation turbulence models. Journal of Geophysical Research 103 (C5), 10543–10554.

Burchard, H., Rippeth, T.P., 2009. Generation of bulk shear spikes in shallow stratified tidal sea. Journal of Physical Oceanography 39, 685–696.

Chen, C., Reid, R.O., Nowlin, W.D., 1996. Near-inertial oscillations off the Texas-Louisiana shelf. Journal of Geophysical Research 101, 3509–3524.

Craig, P.D., 1989a. Constant eddy-viscosity models of vertical structure forced by periodic winds. Continental shelf Research 9, 343–358.

Craig, P.D., 1989b. A model of diurnally forced vertical current structure near 30° latitude. Continental Shelf Research 9, 965–980.

Dale, A.C., Huthnance, J.M., Sherwin, T.J., 2001. Coastal-trapped waves and tides at near-inertial frequencies. Journal of Physical Oceanography 31, 2958–2970.

Danabasoglu, G., Large, W.G., Tribbia, J.J., Gent, P.R., Briegleb, B.P., McWilliams, J.C., 2006. Diurnal coupling in the tropical oceans of CCSM3. Journal of Climate 19, 2347–2365.

De Mesquita, A.R., Harari, J., 2003. On the harmonic constants of tides and tidal currents of the South-eastern Brazilian shelf. Continental Shelf Research, 1227–1237.

DiMarco, S.F., Howard, M.K., Reid, R.O., 2000. Seasonal variation of wind-driven diurnal current on the Texas-Louisiana shelf. Geophysical Research Letters 27 (7), 1017–1020.

Emery, W.J., Thomson, R.E., 1998. Data and Their Analysis Methods in Physical Oceanography. Pergamon Press, Amsterdam, 634 pp.

Furevik, T., Foldvik, A., 1996. Stability at M2 critical latitude in the Barents Sea. Journal of Geophysical Research 101 (C4), 8823–8837.

Gille, S.T., Llewellyn-Smith, S.G., Lee, S.M., 2003. Measuring the sea breeze from QuickSCAT scatterometry. Geophysical Research letters 30, 1114. doi:10.1029/2002GL016230.

Gille, S.T., Lewellyn-Smith, S.G., Statom, N.M., 2005. Global observations of the land breeze. Geophysical Research Letters 32 (5). doi:10.1029/2004GL022139.

Halpern, D., 1977. Description of wind and upper ocean current and temperature variations on the continental shelf off Northwest Africa during March and April 1974. Journal of Physical Oceanography 7, 422–430.

Helland-Hansen, B., Ekman, V.W., 1931. Measurements of ocean currents (experiments in the North Atlantic). Kungliga Fysiografiska Sällskapet i Lund (The Royal Physiographic Society in Lund) 1.

Hyder, P., Simpson, J.H., Christopoulos, S., 2002. Sea breeze forced diurnal surface current in the Thermaikos Gulf, North-west Aegean. Continental Shelf Research 22, 585–601.

Hunter, E., Chant, R., Kohut, J., Bowers, L., Glenn, S., Kohut, J., 2007. Spatial and temporal variability of diurnal wind forcing in the coastal ocean. Geophysical Research Letters 34, 1–5. doi:10.1029/2006GL028945 (L03607).

Jarosz, E., Hallock, Z.R., Teague, W.J., 2007. Near-inertial currents in the DeSoto Canyon region Original Research. Continental Shelf Research 27, 2407–2426.

Jury, M., Spencer-Smith, G., 1988. Doppler sounder observations of trade winds and sea breezes along the African west coast near 34°S, 19°E. Boundary Layer Meteorology 44, 373–405.

Kaplan, D.M., Largier, J.L., Botsford, L.W., 2005. HF radar observations of surface circulation off Bodega Bay (northern California, USA). Journal of Geophysical Research (Oceans) 110 (C10), 1–25. doi:10.1029/2005JC002959 (C10020).

Kaplan, D.M., Largier, J.L., Navarrete, S., Guinez, R., Castilla, J.C., 2003. Large diurnal temperature fluctuations in the nearshore water column. Estuarine, Coastal and Shelf Science 57, 385–398.

Kundu, P.K., Cohen, I.M., 2002. Fluid Mechanics. Academic Press, 730 pp.

Lass, H.U., Mohrholz, V., 2005. On the fluctuations and vertical structure of the shelf circulation off Walvis Bay, Namibia. Continental Shelf Research 25, 1473–1497.

Lerczak, J.A., Hendershott, M.C., Winant, C.D., 2001. Observations and modelling of coastal internal waves driven by a diurnal sea breeze. Journal of Geophysical Research 106 (9), 19,715–19,729.

Lewis, J.K., 2001. Cross-shelf variations of near-inertial current oscillations. Continental Shelf Research 21 (5), 531–543.

Maas, L.R.M., Van Haren, J.J.M., 1987. Observations on the vertical structure of tidal and inertial currents in the central North Sea. Journal of Marine Research 45, 293–318.

Middleton, J.H., Denniss, T., 1993. The propagation of tides near the critical latitude. Geophysical and Astrophysical Fluid Dynamics 68, 1–13.

Munk, W., Wunsch, C., 1998. Abyssal recipes II: energetics of tidal and wind mixing. Deep-Sea Research I 45, 1977–2010.

Park, J., Kim, K., King, B., 2005. Global statistics of inertial motions. Geophysical Research Letters 32, 1–5. doi:10.1029/2005GL023258 (L14612).

Pattiaratchi, C., Hegge, B., Gould, J., Eliot, I., 1997. Impact of sea-breeze activity on nearshore and foreshore processes in southwestern Australia. Continental Shelf Research 17, 1539–1560.

Pidgeon, E.J., Winant, C.D., 2005. Diurnal variability in currents and temperature on the continental shelf between central and southern California. Journal of Geophysical Research 110, 13 pp. doi:10.1029/2004JC002321 (C03024).

Pinones, A., Valle-Levinson, A., Narvaez, D.A., Vargas, C.A., Navarrete, S.A., Yuras, G., Castilla, J.C., 2005. Wind-induced diurnal variability in river plume motion. Estuarine, Coastal and Shelf Science 65, 513–525.

Pollard, R.T., 1970. On the generation by winds of inertial waves in the ocean. Deep-Sea Research 17, 795–812.

Pollard, R.T., 1980. Properties of near-surface Inertial Oscillations. Journal of Physical Oceanography 10, 385–397.

Pollard, R., Millard, R., 1970. Comparison between observed and simulated wind generated inertial oscillations. Deep-Sea Research 17, 813–821.

Poulain, P.M., 1990. Near-inertial and diurnal motion in the trajectories of mixed layer drifters. Journal of Marine Research 48, 793–823.

Preston-Whyte, R.A., Tyson, P.D., 1988. The Atmosphere and Weather of Southern Africa. Oxford University Press, Cape Town, 374 pp.

Price, J.F., 1981. On the upper ocean response to a moving hurricane. Journal of Physical Oceanography 11, 153–175.

Pugh, D.T., 1987. Tides, Surges and Mean Sea Level. John Wiley and Sons Ltd., 472 pp.

Reynolds-Fleming, J.V., Luettich, R.A., 2004. Wind driven lateral variability in a partially mixed estuary. Estuarine, Coastal and Shelf Science 60, 395–407.

Rippeth, T.P., Simpson, J.H., Player, R.J., Garcia, M., 2002. Current oscillations in the diurnal inertial band on the Catalonian Shelf in Spring. Continental Shelf Research 22, 247–265.

Rosenfeld, L.K., 1988. Diurnal period wind stress and current fluctuations over the continental shelf of northern California. Journal of Geophysical Research 93, 2257–2276.

Rotunno, R., 1983. On the linear theory of the land and sea breeze. Journal of the Atmospheric Sciences 40 (8), 1999–2009.

Schahinger, R.B., 1988. Near-inertial motion on the South Australian Shelf. Journal of Physical Oceanography 18, 492–504.

Simionato, C.G., Meccia, V., Dragani, W., Nunez, M., 2005. Barotropic tide and baroclinic waves observations in the Rio de la Plata Estuary. Journal of Geophysical Research 110, 1–16. doi:10.1029/2004JC002842 (C06008).

Simmons, H.L., 2008. Spectral modification and geographic redistribution of the semi-diurnal internal tide. Ocean Modelling 21, 126–138.

Simmons, H.L., Hallberg, R., Arbic, B., 2004. Internal wave generation in a global baroclinic tide model. Deep-Sea Research II 51, 3042–3068.

Simpson, J.E., 1994. Sea Breeze and Local Wind. Cambridge University Press, 234 pp.

Simpson, J.H., Hyder, P., Rippeth, T.P., Lucas, I., 2002. Forced oscillations near the critical latitude for diurnal inertial resonance. Journal of Physical Oceanography 32, 177–187.

Sobarzo, M., Bravo, L., Moffat, C., 2010. Diurnal-period, wind-forced ocean variability on the inner shelf off Concepción, Chile. Continental Shelf Research 30, 2043–2056.

Umlauf, L., Burchard, H., Bolding, K., 2007. General Ocean Turbulence Model (GOTM) Source code and Test Case Documentation—Version 4.0, online manual 〈www.gotm.net〉, 376 pp.

Van Haren, H., 2005. Tidal and near-inertial peak variations around the diurnal critical latitude. Geophysical Research Letters 32, L23611. doi:10.1029/2005GL024160.

Walsh, J.E., 1974. Sea breeze theory and applications. Journal of Atmospheric Sciences 31, 2012–2026.

Watanabe, M., Hibiya, T., 2002. Global estimates of the wind-induced energy flux to inertial motions in the surface mixed layer. Geophysical Research Letters 29 (8). doi:10.1029/2001GL014422.

Xing, J., Chen, R., Proctor, R., 1999. A two-dimensional slice model of the shelf edge region off the west coast of Scotland: model response to realistic seasonal forcing and the role of the M2 tide. Continental Shelf Research 19, 1353–1386.

Xing, J., Davies, A.M., Fraunie, P., 2004. Model studies of near-inertial motion on the continental shelf off northeast Spain: a three-dimensional/two-dimensional/one-dimensional model comparison study. Journal of Geophysical Research 109, C01017. doi:10.1029/2003JC001822.

Yelland, M., Taylor, P.K., 1996. Wind stress measurements from the open ocean. Journal of Physical Oceanography 26, 541–558.

Yelland, M.J., Moat, B.I., Taylor, P.K., Pascal, R.W., Hutchings, J., Cornell, V.C., 1998. Wind stress measurements from the open ocean corrected for airflow distortion by the ship. Journal Physical Oceanography 28, 1511–1526.

Zavialov, P., Moller, O., Campos, E., 2002. First direct measurements of currents on the continental shelf of Southern Brazil. Continental Shelf Research 22, 1975–1986.

Zhang X., DiMarco, S.F., Smith D.C. IV, Howard, M.K., Jochens, A.E., Hetland, R.D., 2009. Near-resonant ocean response to sea breeze on a stratified Continental Shelf. Journal of Physical Oceanography, 39, 2137–2155.

Zhang, X., Smith IV, D.C., DiMarco, S.F., Hetland, R.D., 2010. A numerical study of sea-breeze-driven ocean poincare wave propagation and mixing near the critical latitude. Journal of Physical Oceanography 40, 48–66.